



HAL
open science

Influence of dislocations on hydrogen diffusion and trapping in an Al-Zn-Mg aluminium alloy

Loïc Oger, Benoît Malard, Grégory Odemer, Lionel Peguet, Christine Blanc

► **To cite this version:**

Loïc Oger, Benoît Malard, Grégory Odemer, Lionel Peguet, Christine Blanc. Influence of dislocations on hydrogen diffusion and trapping in an Al-Zn-Mg aluminium alloy. *Materials & Design*, 2019, 180, pp.1-11. 10.1016/j.matdes.2019.107901 . hal-02883849

HAL Id: hal-02883849

<https://hal.science/hal-02883849>

Submitted on 29 Jun 2020

HAL is a multi-disciplinary open access archive for the deposit and dissemination of scientific research documents, whether they are published or not. The documents may come from teaching and research institutions in France or abroad, or from public or private research centers.

L'archive ouverte pluridisciplinaire **HAL**, est destinée au dépôt et à la diffusion de documents scientifiques de niveau recherche, publiés ou non, émanant des établissements d'enseignement et de recherche français ou étrangers, des laboratoires publics ou privés.







Open Archive Toulouse Archive Ouverte (OATAO)

OATAO is an open access repository that collects the work of Toulouse researchers and makes it freely available over the web where possible

This is a Publisher's version published in: <http://oatao.univ-toulouse.fr/24132>

Official URL: <https://doi.org/10.1016/j.matdes.2019.107901>

To cite this version:

Oger, Loïc  and Malard, Benoît  and Odemer, Grégory  and Peguet, Lionel and Blanc, Christine  *Influence of dislocations on hydrogen diffusion and trapping in an Al-Zn-Mg aluminium alloy.* (2019) *Materials & Design*, 180. 1-11. ISSN 0264-1275

Any correspondence concerning this service should be sent to the repository administrator: tech-oatao@listes-diff.inp-toulouse.fr



Influence of dislocations on hydrogen diffusion and trapping in an Al-Zn-Mg aluminium alloy

L. Oger^{a,b}, B. Malard^a, G. Odemer^a, L. Peguet^b, C. Blanc^{a,*}

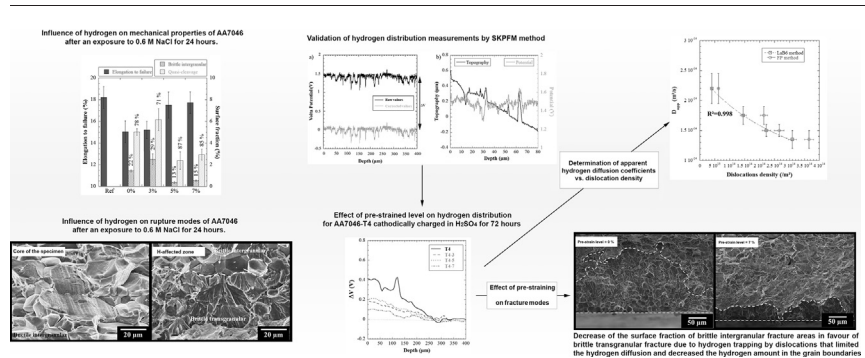
^a CIRIMAT, Université de Toulouse, CNRS, INPT-ENSIACET, 4 Allée Emile Monso, BP 44362, 31030 Toulouse Cedex 4, France

^b Constellium Technology Center, 725 rue Aristide Bergès, CS 10027, 38341 Voreppe cedex, France

HIGHLIGHTS

- The higher the density of motionless dislocations, the lower the H-induced elongation to failure loss.
- H trapping by motionless dislocations limited H diffusion and decreased the H amount at grain boundaries.
- H trapping by motionless dislocations promoted a brittle transgranular fracture.

GRAPHICAL ABSTRACT



ARTICLE INFO

Article history:

Received 29 March 2019

Received in revised form 18 May 2019

Accepted 28 May 2019

Available online 01 June 2019

Keywords:

Aluminium alloy

Automotive industry

Hydrogen embrittlement

Hydrogen-dislocation interactions

Hydrogen trapping

ABSTRACT

Cu-lean Al-Zn-Mg alloys are known to be susceptible to hydrogen embrittlement (HE), which currently limits their use in automotive industry. Several works suggested that the resulting loss of mechanical properties was related to hydrogen trapping in different metallurgical sites. The present work attempts to provide a better understanding of the hydrogen-dislocations interactions to evaluate their influence on the loss of mechanical properties of hydrogen-embrittled Al-Zn-Mg alloys. Pre-strained samples of 7046 aluminium alloy (AA7046) were therefore prepared in order to increase the density of motionless dislocations. Tensile samples, pre-strained or not, were then corroded in 0.6 M NaCl and mechanically tested to evaluate their HE susceptibility and the role of dislocations on hydrogen diffusion. Results highlighted a significant improvement of the HE resistance of the alloy with the increase in the density of motionless dislocations induced by the pre-strain step. This was attributed to preferential hydrogen trapping on motionless dislocations leading to a decrease in the hydrogen amount in the grain boundaries. The measurements of hydrogen penetration depth by Scanning Kelvin Probe Force Microscopy (SKPFM) for cathodically charged samples provided further evidence to support these assumptions.

© 2019 The Authors. Published by Elsevier Ltd. This is an open access article under the CC BY-NC-ND license (<http://creativecommons.org/licenses/by-nc-nd/4.0/>).

1. Introduction

Al-Zn-Mg alloys are known to be the age-hardenable aluminium alloys with the highest mechanical properties. Due to their low density, they are nowadays increasingly considered as the best alternative to replace steels as structural components in automotive

* Corresponding author at: CIRIMAT, Université de Toulouse, CNRS, INPT-ENSIACET, 4 allée Emile Monso, BP 44362, 31030 Toulouse cedex 4, France.

E-mail address: christine.blanc@ensiacet.fr (C. Blanc).

industry according to recent environmental requirements [1]. However, their susceptibility to stress corrosion cracking (SCC) observed for some conditions is a limiting factor [2–4]. Generally, cracks are initiated from surface heterogeneities related to elaboration processes or from corrosion defects (pitting or intergranular corrosion). These local defects can then evolve into crack embryos according to different types of damage mechanisms, such as preferential dissolution of the grain boundaries when the alloy is susceptible to intergranular corrosion, stress concentration at the tip of the surface heterogeneities, or hydrogen absorption in the alloy, which promotes a decrease in the cohesion stresses [5]. Concerning the 7xxx series aluminium alloys, authors generally recognise the predominant role of hydrogen embrittlement (HE) during SCC mechanisms [2,3,5,6]. This phenomenon is generally characterised for 7xxx aluminium alloys by a loss of the elongation to failure [7,8], and brittle intergranular and transgranular fracture modes in relation with a hydrogen-induced decrease in the intergranular and interplanar cohesion stresses [9]. This behaviour can be related to different hydrogen trapping sites, firstly evocated by Pressouyre [10] and classified as reversible traps, such as dislocations [11], vacancies and low-angle grain boundaries [12] or as irreversible traps, such as precipitates/matrix interfaces [13] and high-angle grain boundaries [14]. More specifically, over the last decades, the studies on this topic offered many models based on hydrogen-plasticity interactions to explain HE mechanisms. The specific operative mechanism depends on the type of material, the environment and the loading conditions. Among the proposed mechanisms, the most evocated are:

- The adsorption-induced dislocation emission (AIDE) model [15], which supposes hydrogen adsorption in the first atomic layers of the alloy leading to the emission of dislocations from the top of the defect;
- The hydrogen-enhanced localised plasticity (HELP) model [16], which suggests the presence of hydrogen in the Cottrell atmosphere of dislocations leading finally to enhance localised plasticity.

These models are based on the following observations:

- A decrease in the elastic interactions between dislocations highlighted by transmission electron microscopy observations in a 310S steel, which showed a decrease in the distance between dislocations in the presence of hydrogen [17];
- A hydrogen effect on dislocation mobility in 7075, 7050 and high-purity aluminium alloys [18,19];
- An inhibition of the dislocation cross-slip leading to dislocation piling [20,21].

However, few studies focused on how hydrogen trapped on specific microstructural sites affects the mechanical properties and the fracture mode for 7xxx aluminium alloys. A previous study concerned hydrogen trapping on hardening precipitates in such an alloy [22]. In order to broaden the understanding of the overall mechanisms, the present work attempts to provide a better insight of hydrogen-dislocations interactions and their role on the loss of mechanical properties. Hydrogen trapping by motionless dislocations was investigated by measuring the loss in mechanical properties for pre-strained samples of a 7046 aluminium alloy (AA7046) after an exposure to chloride media in order to simulate SCC environment. The results were completed by studying AA7046 samples that had been pre-strained by tensile tests and then hydrogen-charged in a pH 2 H_2SO_4 solution. For these samples, the hydrogen penetration depth was determined by Scanning Kelvin Probe Force Microscopy (SKPFM). This technique emerges as one possible solution to detect hydrogen at room temperature [23–25].

2. Experimental procedure

2.1. Material and specimen preparation

2.1.1. Material and microstructure characterisation

The AA7046 (Al base, 6.6–7.6% Zn, 1.0–1.6% Mg, <0.25 Cu, wt%) was provided as 2 mm thick sheets in the T4 state, i.e. hot rolled, cold rolled, solution heat treated and then stored at room temperature until substantially stable. Coarse intermetallic particles were characterised by optical microscopy (OM Olympus PMG3) and by scanning electron microscopy (SEM LEO435VP) coupled with Energy Dispersive X-ray Spectroscopy (EDS IMIX analyser) technique.

2.1.2. Tensile specimen preparation

Flat tensile samples were machined in the 2 mm thick sheet by using an electro-erosion process leading to the geometry shown in Fig. 1. Before the tests, they were mechanically abraded with SiC paper (grade 1200) to remove the zone affected by the electro-erosion process (100 μm removed), then polished with 9 μm and 3 μm diamond paste, rinsed during 30 s in an ultrasonic bath and finally air-dried. Distilled water was used as a lubricant for all these steps.

2.1.3. Pre-strain stage

The AA7046-T4 tensile samples were pre-strained prior to exposure to NaCl solution or cathodic hydrogen charging in order to increase the density of motionless dislocations. The pre-straining step was performed by tensile tests at a constant strain rate of $10^{-3} s^{-1}$ at room temperature. The tests were interrupted at specified strain levels, i.e. 3, 5 and 7% of total strain. For a pre-strain level of 10%, small cracks formed on the sample surface, which could modify the corrosion behaviour of AA7046 during the immersion in chloride solution or during hydrogen charging in sulfuric acid. So, it was decided not to exceed 7% of total strain level in this work.

In the following, the pre-strain level is quantified considering the total strain, i.e. elastic and plastic deformation. In order to simplify the notations, the samples were called as T4, T4-3, T4-5 and T4-7 referring to the total strain applied, respectively 0, 3, 5 and 7%. The microstructural changes due to the pre-strain stage were evaluated by X-Ray Diffraction measurements as described in Section 2.4.

2.2. Hydrogen charging and hydrogen penetration depth measurements

As explained, the aim of this study was to evaluate the role of dislocations on hydrogen diffusion and trapping in the alloy and finally the loss of mechanical properties for hydrogen-embrittled samples. Several

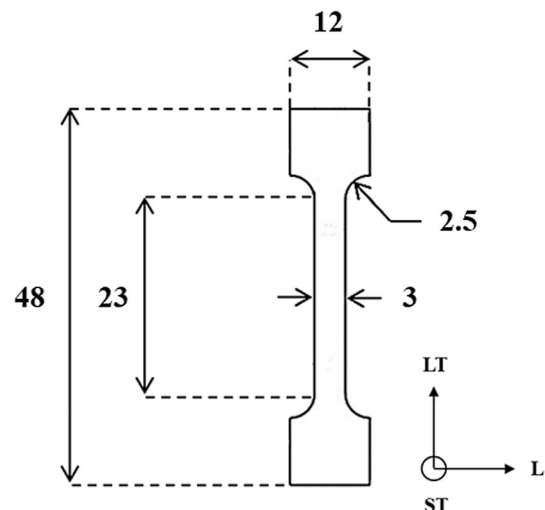


Fig. 1. Geometry of tensile samples (dimensions in mm).

works reported a hydrogen intake during exposure in chloride media due to the corrosion processes, which was confirmed by preliminary experiments. So, in the present work, some experiments were therefore performed for samples enriched in hydrogen following an exposure to a chloride solution. However, other samples were prepared by using cathodic hydrogen charging in sulfuric acid in order to distinguish between the effects of hydrogen and those induced by corrosion processes. Further, this charging method allowed to obtain a homogeneous distribution of hydrogen inside the samples in contrast to the heterogeneous distribution of hydrogen produced by localised corrosion mechanisms in NaCl solution.

2.2.1. For tensile tests: hydrogen charging by immersion in chloride solution

The loss of mechanical properties induced by hydrogen was evaluated by performing tensile tests for samples previously immersed in a 0.6 M NaCl solution for 24 h. In this case, only the gauge length of the tensile samples was exposed to the chloride solution, the heads and the edges being protected by silicone. The temperature of both the laboratory room and the electrolyte was controlled and maintained at 25 °C. Such a charging method led to the penetration of hydrogen around the corrosion sites, i.e. to a heterogeneous hydrogen distribution but with a hydrogen amount large enough to generate a decrease in the mechanical properties and a modification of the fracture modes. Global hydrogen amount measurements were carried out by using a melting method.

2.2.2. For SKPFM measurements: hydrogen charging by cathodic polarisation in H₂SO₄

The hydrogen penetration depth was measured by SKPFM measurements, which requires a homogeneous distribution of hydrogen in the plane perpendicular to the hydrogen flow. Therefore, samples were cut from the pre-strained tensile samples and machined as parallelepipeds of 15 (L) × 3 (LT) × 2 (ST) mm³ (L: longitudinal, LT: long transverse and ST: short transverse). Hydrogen was introduced by cathodic charging at 25 ± 2 °C in a pH 2 H₂SO₄ solution. During cathodic charging, only the L-LT plane was exposed to the electrolyte, all other planes being protected by a transparent lacquer and a silicone layer. A three-electrode system with a Pt counter electrode and a saturated calomel electrode (SCE) as reference was used to apply a potential of -1.450 V vs SCE for 72 h. This cathodic potential was chosen to optimise the hydrogen penetration [22].

2.2.3. Measurements of the hydrogen penetration depth by SKPFM

SKPFM measurements were performed on a 5500 Agilent Atomic Force Microscope (AFM). Previous results showed that this method is particularly adapted to study the hydrogen diffusion in aluminium alloys [22,26]. Because the measurements are performed at room temperature, this technic avoids any risk of changes in the microstructure observed for the aluminium alloys at temperatures higher than 100 °C, which limits the use of the classical thermal desorption spectroscopy (TDS) method. AFM was used in the single pass mode, meaning that both topography and surface potential signals were acquired simultaneously. Conductive Pt-coated silicon tips were used as probes. With this set up, the tip vibrates above the surface at two different frequencies: a mechanical excitation close to the resonant frequency of the tip controls the tip-surface distance and an electrical excitation allows a surface potential to be measured [27]. A spatial resolution of approximately 50 nm [24] was obtained using the amplitude modulation mode also called (AM)-KFM. In this configuration, an oscillating potential difference ($V_{dc} - V_{ac} \sin(\omega t)$) is applied between the tip and the sample surface. This modulates the electrostatic forces induced by the decrease in the distance between the tip and the sample leading to the oscillation of the tip. The surface potential corresponds to the value of V_{dc} when the oscillations are minimal. Admitting that the surface potential measured is related to the electronic output work, it was suggested that hydrogen in the lattice could modify it [28]. A

previous work largely demonstrated that the presence of hydrogen in the AA7046 led to an increase in the surface potential, attributed to a local distortion of the lattice [22].

In this study, after hydrogen charging in sulfuric acid (L-LT plane exposed to H₂SO₄), the samples were polished parallel to the LT-ST plane with 1/4 μm diamond paste to remove approximately 500 μm. Then, the SKPFM measurements were conducted in the LT-ST plane of the sample: successive rectangular sections of 80 μm × 6 μm were scanned from the hydrogen-charged surface up to 400 μm in the core of the sample in the ST direction. The different sections were matched by comparison of the topographic maps. Results were analysed with the Gwyddion software. The time between charging and SKPFM measurements was estimated to be 20 min.

2.3. Evaluation of the tensile mechanical properties for hydrogen-charged samples

For hydrogen-charged samples following an exposure to NaCl solution, tensile tests were carried out at a strain rate of 10⁻³ s⁻¹ at room temperature in air with a dual column MTS testing machine (frame capacity of 30 kN). The strain was measured by means of a contact extensometer. The results obtained for hydrogen-charged samples were compared to those for hydrogen-free samples to highlight the effects of hydrogen on the mechanical properties. The time between the end of hydrogen charging in NaCl solution and the beginning of the tensile tests was maintained constant, i.e. 20 min: it corresponded to the time required from an experimental point of view. Hydrogen desorption during such a short time was assumed to be negligible. SEM was used to observe the fracture surfaces of the samples after tensile tests.

2.4. X-ray diffraction measurements

X-ray diffraction (XRD) measurements were carried out by using a Bruker D8 Discover diffractometer equipped with a copper source to evaluate the dislocation density for pre-strained samples. Two methods were carried out to evaluate the pseudo-Voigt peak broadening related to the instrument configuration. This allowed the deconvolution of the signal due to the instrumental configuration on one hand, and to the physical parameters (crystallite size and microstrain) on the other hand. The first method consisted in analysing a LaB₆ standard powder sample from the National Institute of Standards and Technology (NIST). This standard is calibrated and supposed to have a large crystallite size and no microstrain, leading to minimise the influence of these physical parameters on the signal obtained from this sample. With this method, the Caglioti parameters (U, V, W for Gaussian components and X, Y for the Lorentz components) were obtained. The second method was based on Fundamental Parameters (FP), which corresponds to the description of the instrumental configuration implemented in the TOPAS software [29].

After the calibration, measurements were performed on pre-strained samples (15x3x2 mm³) at room temperature with a θ - θ mounting, from $2\theta = 20^\circ$ to 120° , with a step of 0.05° for an acquisition time of 8 s per point. The crystallite sizes (Lorentz contribution) and the microstrain (Gaussian contribution) were determined for each sample using the Topas software [29] built to achieve the Rietveld Method [30].

3. Results and discussion

3.1. Dislocation density

Microstructural evolutions induced by the pre-strain stage, i.e. changes in the dislocation density, were not directly observed by transmission electron microscopy (TEM) but were evaluated by XRD measurements. This method was preferred at first because TEM sample preparation can induce a decrease in the density of dislocations in the near surface [31]; further, TEM observations can only bring data for a

small volume. On the contrary, XRD allowed a volume ($20 \text{ mm} \times 10 \text{ mm} \times 0.05 \text{ mm} = 10 \text{ mm}^3$) more representative of the global microstructure to be analysed. Using the two methods described above, the lattice parameter, the crystallite size and the microstrain were determined for each pre-strained sample; the results are summarised in Table 1. They exhibit a decrease in the average crystallite size when the pre-strain level increases in relation with the formation of a dislocation network in the microstructure. As a consequence, the resulting microstrain between crystallites increases when the pre-strain level increases.

Based on these measurements, the dislocation density ρ was calculated using the relationship proposed by Williamson and Smallman [32,33]:

$$\rho = \frac{2\sqrt{3}\epsilon}{Db} \quad (1)$$

where ϵ is the microstrain, D corresponds to the crystallite size and b is the Burger's vector ($b = \frac{a}{\sqrt{2}}$ in fcc structure with a the lattice parameter). Fig. 2 shows an increase in the dislocation density when the macroscopic strain applied increases. A linear evolution can be noticed, which is consistent with literature results. Adachi et al. [34] studied the influence of the grain size for a 1100 aluminium alloy on the evolution of the dislocation density during in-situ tensile tests. They reported a 4-stage evolution related to elastic, micro-plastic, plastic and pre-failure strain. The pure elastic strain led to a non-significant change of the dislocation density explained by the absence of dislocation formation during this step. In the micro-plastic domain, dislocations could nucleate in grains with a preferential orientation in relation with the macroscopic load applied. This led to a strong increase in the dislocation density. During plastic deformation, the dislocation density followed a linear evolution versus the strain up to the necking before failure. During this third step, the slope of the dislocation density vs strain straight line increased with the grain size. Concerning the specific case of the AA7046 studied in this work, the grain size should promote a strong increase in the dislocation density in the plastic deformation domain, consistent with the measurements. By the way, the order of magnitude of 10^{14} – 10^{15} m^{-2} calculated for the dislocation density was also consistent with the values obtained for similar strain levels in the literature [34,35].

3.2. Effect of pre-strain on tensile properties and fracture modes

The hydrogen/dislocations interactions were first studied for pre-corroded samples, i.e. hydrogen-charged in 0.6 M NaCl solution. Preliminary tests showed that a 24-h immersion in this electrolyte led to a hydrogen enrichment of approximately 23 wppm for all samples, independent of the pre-strain level. OM observations of the sample surface showed that the morphology of the corrosion was the same for the four strain states, i.e. dissolution of the matrix around coarse intermetallic particles (black round spots in Fig. 3). For a longer immersion time (72 h), a few pits were observed; they propagated from these sites (results not shown here). Cross-sections showed only a slight propagation of the corrosion defects ($<30 \mu\text{m}$) for a 24-hour immersion and no intergranular defect was observed. Considering the similar corrosion defect morphology for all samples, it was assumed that their HE susceptibility could be compared.

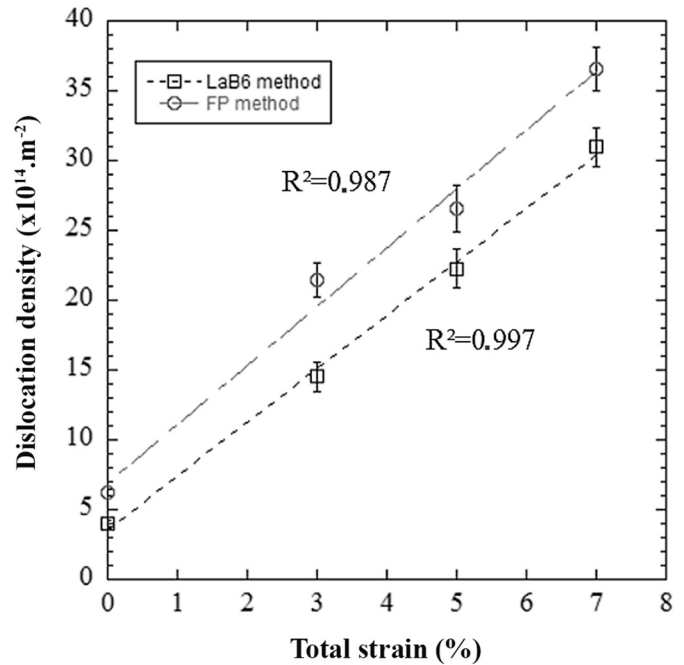


Fig. 2. Dislocation density versus total strain in AA7046 samples obtained by calculations based on XRD measurements.

The results of the tensile tests performed for pre-strained samples after a 24-hour exposure to the NaCl solution are presented in Fig. 4. The reference corresponds to the mechanical properties of the AA7046-T4 which was not pre-strained and not exposed to the corrosive environment. A significant decrease in the elongation to failure was measured for corroded T4 and T4-3 samples by comparison to the reference sample, which was attributed to corrosion-induced hydrogen embrittlement in agreement with the literature [3]. On the opposite, when the pre-strain level was higher, i.e. for the T4-5 and T4-7 samples, the loss of mechanical properties was less noticeable.

These measurements were completed by fracture surface observations for the pre-corroded samples. Fig. 5 shows SEM observations of the fracture surfaces in the core of the sample, non-affected by hydrogen (Fig. 5a), and in the hydrogen-affected zone (Fig. 5b) for an AA7046 T4 sample which was not pre-strained. Results showed that the alloy was characterised by ductile intergranular fracture mode in the absence of hydrogen (Fig. 5a) whereas it exhibited brittle intergranular and brittle transgranular (quasi-cleavage) fracture areas (Fig. 5b) when it was embrittled by hydrogen. This was in good agreement with a previous study showing that, for the AA7046, when hydrogen was present inside the alloy, it localised preferentially in the grain boundaries leading to a decrease in the intergranular cohesion stresses and then to brittle intergranular fracture [26]. Quasi-cleavage fracture was also observed when the hydrogen amount in the grain boundaries was not sufficient enough to promote the crack propagation in the grain boundaries. Similar fracture surfaces were observed for all pre-strained samples. However, a global observation of the fracture surfaces

Table 1

Calculated values of crystallite size and heterogeneous strain for AA7046 samples at different levels of total strain. Values obtained from XRD measurements.

Total strain (%)	LaB6			FP		
	Lattice parameter (Å)	Crystallite size (nm)	Heterogeneous microstrain (%)	Lattice parameter (Å)	Crystallite size (nm)	Heterogeneous microstrain (%)
0	4.0554 ± 0.0003	392 ± 14	0.129 ± 0.002	4.0557 ± 0.0003	251 ± 5	0.129 ± 0.002
3	4.0528 ± 0.0013	254 ± 12	0.305 ± 0.007	4.0536 ± 0.0027	179 ± 6	0.318 ± 0.007
5	4.0526 ± 0.0016	183 ± 7	0.337 ± 0.008	4.0528 ± 0.0015	148 ± 5	0.325 ± 0.009
7	4.0524 ± 0.0020	153 ± 4	0.392 ± 0.007	4.0527 ± 0.0024	127 ± 3	0.384 ± 0.007

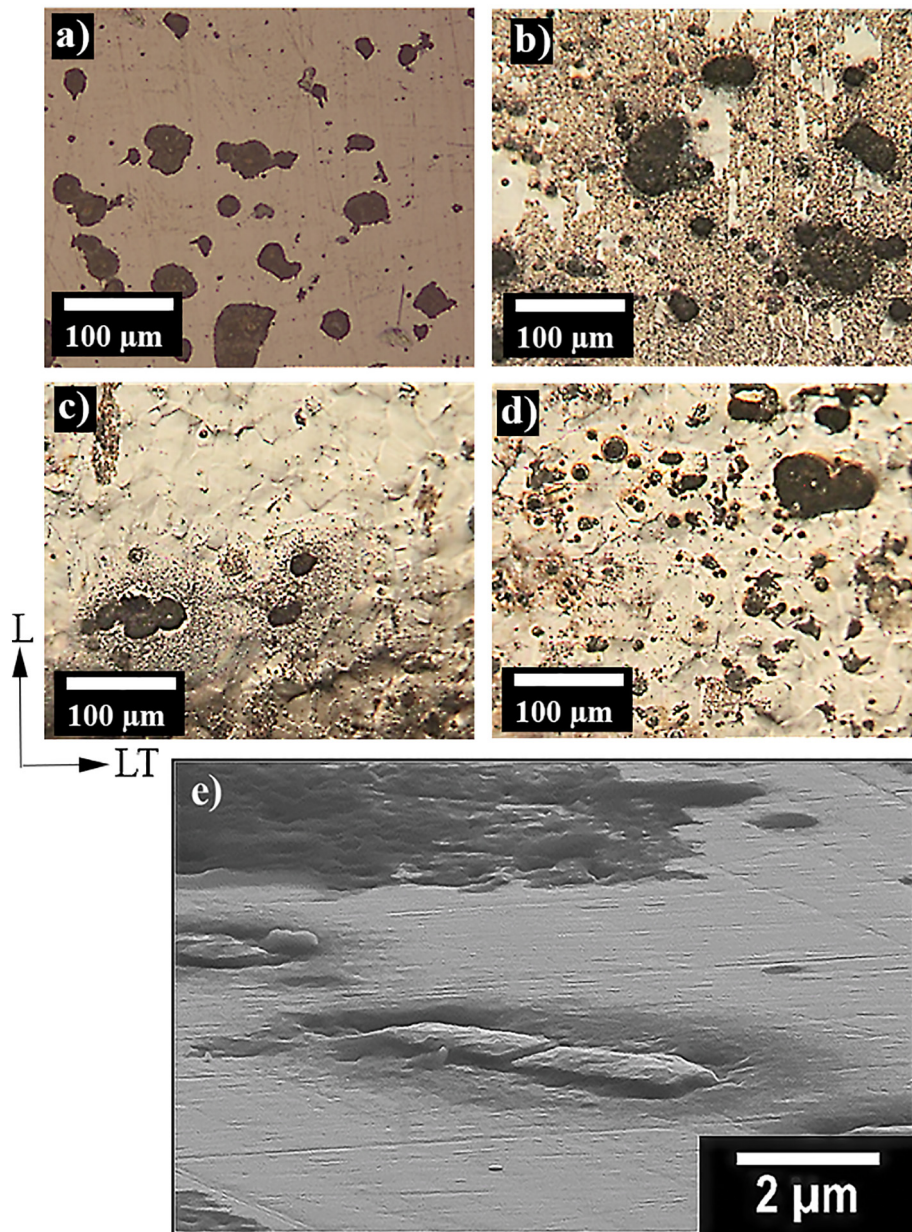


Fig. 3. OM micrographs of the pre-strained AA7046 samples exposed for 24 h in 0.6 M NaCl. Pre-strain level equal to 0% (a), 3% (b), 5% (c) and 7% (d). (e) SEM (secondary electrons) observations of a T4-3 sample after exposure to NaCl.

suggested that T4 (Fig. 5c) and T4-3 (Fig. 5d) samples showed deeper brittle areas than the T4-5 (Fig. 5e) and T4-7 (Fig. 5f) samples.

Then, the fraction of surface area corresponding to each brittle fracture mode, i.e. intergranular or quasi-cleavage, was calculated with the ImageJ software on the basis of SEM observations (Fig. 4). Results showed that the total fraction of surface area corresponding to brittle fracture mode varied with the total pre-strain level. More precisely, it was quite similar for T4 and T4-3 samples, considering the error bars, but was significantly lower for T4-5 and T4-7 samples. It was also noticeable that brittle intergranular zones were less extended on T4-5 and T4-7 compared to T4 and T4-3 samples. Globally, these changes were well-correlated with the evolution of the elongation to failure versus the pre-strain level. Clearly, the sole analysis of the fracture surfaces was not sufficient to explain the HE susceptibility of the AA7046, in particular because the fraction of surface area corresponding to brittle fracture mode could not be directly related to the hydrogen diffusion inside the alloy. Nevertheless, the results suggested interactions between hydrogen and the alloy microstructure.

More precisely, the results could be explained by considering that corrosion-induced hydrogen could be preferentially trapped on motionless dislocations generated during the pre-strain stage, limiting both its penetration depth and its location in grain boundaries. This could explain why an increase in the total strain led to a decrease in the brittle surface area, on the one part, and, in particular, in the surface area corresponding to brittle intergranular zones, on the other part, as observed in T4-5 and T4-7 states. In T4 and T4-3 samples, the total strain was probably too low so that the limitation of hydrogen diffusion by the dislocations could not be highlighted with this method. As previously explained, these results did not allow the hydrogen penetration depth to be determined with accuracy: therefore, further SKPFM measurements were performed before discussing the results.

Moreover, it was also of interest to consider the internal stresses induced by the pre-strain stage due to the strain incompatibilities between grains with different crystallographic orientations. When the pre-strain level increased, plastic deformation concerned more and more grains leading to a redistribution of the internal stresses. Clearly,

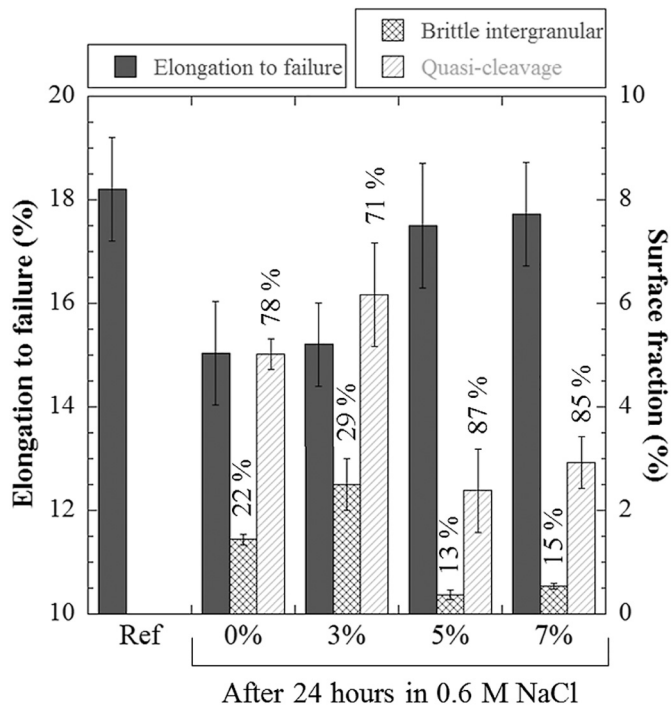


Fig. 4. Elongation to failure of pre-strained samples after an exposure to 0.6 M NaCl for 24 h. The fractions of surface area corresponding to each fracture mode and evaluated by SEM observations are also given for all pre-strained samples after the exposure to NaCl solution. The percentages over the bars correspond to the proportions of brittle intergranular and quasi-cleavage areas considering the brittle hydrogen-affected zone. The reference sample was not pre-strained and not exposed to the NaCl solution.

the internal stresses could be assumed to promote the HE susceptibility of the alloy with a particular susceptibility of the grain boundaries whereas, in parallel, the increase in the density of dislocations with the pre-strain stage could be helpful in protecting the alloy towards brittle fracture with hydrogen trapping in the dislocation network. Therefore, two elementary mechanisms could be considered that competed with each other. For T4-3 samples, the dislocation density was too low to inhibit the effect of the internal stresses. On the contrary, for T4-5 and T4-7 samples, the dislocation network could promote efficiently hydrogen trapping and therefore it could limit hydrogen diffusion towards the grain boundaries leading to a decrease in the fraction of surface area corresponding to brittle intergranular fracture.

3.3. Effect of pre-strain on hydrogen diffusion

Additional measurements were carried out in order to complete previous observations and to bring some quantitative data related to hydrogen diffusion. In a previous work that focused on hydrogen-hardening precipitates interactions, SKPFM was shown to be relevant and adapted to study the hydrogen diffusion in 7xxx aluminium alloys. Indeed, Volta potential values were shown to be affected by hydrogen so that Volta potential measurements allowed to determine precisely the hydrogen penetration depth from the hydrogen-charged surface to the core of the specimens [22]. Similar measurements were carried out in the present work. To take into account a change in environmental conditions, i.e. a change in relative humidity, even though this parameter was controlled in the room, all Volta potential values were normalised by calculating ΔV , which corresponded to the difference between the potential in the uncharged part of the sample, very far from the charging side, V_∞ , and the measured potential at a distance x , V_x . Fig. 6a shows the normalised Volta potential, ΔV , obtained from the raw values for an uncharged sample as a function of the distance from the surface. The potential remained stable from the surface up to the core of the specimen, and, due to the definition, ΔV was therefore

equal to zero. No meaningful change was observed all along the profile except for local peaks that were attributed to interactions between the tip and the coarse intermetallics. Indeed, Fig. 6b shows that, when the Pt-coated silicon tip was above an intermetallic particle (zones 2 and 3), the Volta potential increased or decreased, probably depending on the nature of the particles (Al_3Fe or Al_3Ti according to SEM observations and EDX characterisations). On the opposite, when the topography presented variations due to the surface roughness but no composition change (1), no change of the Volta potential could be observed. It could thus be concluded that the SKPFM measurements depended on the substrate microstructure, which was in good agreement with the works of Senöz et al [24,28] who suggested that the change in potential detected by SKPFM was related to a local electrochemical equilibrium at the surface [28]. A thin film of water would form on the sample surface and the hydrogen, that would have previously penetrated in the sample, would desorb in this film and would be oxidised. However, this explanation could only bring evidences for the presence of untrapped hydrogen. The changes in the electronic work function induced by trapped hydrogen had to be related to other parameters. In fact, it could be considered that trapped hydrogen induced a change in the local relaxation of the subsurface, leading to a local modification of the atomic three-dimensional arrangement. This could explain (as observed for the coarse intermetallics) the modification of the electronic work function and thus of the Volta potential measured in the presence of trapped hydrogen. This idea is supported by the works of Fusy et al. [36] on the influence of the oxygen adsorption on rhenium; the authors showed a superficial rearrangement of the rhenium surface when a critical concentration of oxygen was reached in the subsurface. This rearrangement was also related to a modification of the electron work function. Clearly, in the presence of a hydrogen gradient inside the material, a ΔV gradient was therefore expected whereas, in the presence of coarse intermetallics, only local ΔV variations were expected, as shown by the peaks previously observed (Fig. 6b).

Fig. 7 shows SKPFM measurements on hydrogen-charged samples. It highlights ΔV gradients from the hydrogen-charged surface (i.e. 0 μm) up to the core of the samples (i.e. max 400 μm). Assuming that the areas with a higher Volta potential (and thus a higher electronic work function) corresponded to the zones affected by hydrogen, it was thus possible to determine a hydrogen penetration depth from the SKPFM curves. It was considered that the maximal hydrogen penetration depth d_H^{exp} was reached when the weighted moving average was lower to 20 mV compared to the average magnitude of the Volta potential variations. This method was shown to be effective in a previous work [22]. On the basis of this methodology, a slight decrease in the hydrogen penetration depth was noticed when the total pre-strained level increased. This observation suggested that the hydrogen diffusion was slowed down due to plastic deformation, which was attributed to the increase in the density of motionless dislocations.

In order to highlight the differences between all pre-strained samples, the apparent hydrogen diffusion coefficient, D_{app} , was estimated by using the second Fick's law solution (Eq. (2)). It was considered that:

- The hydrogen concentration at the surface during the charging, C_s , was constant, with $C_s = 1$;
- The hydrogen concentration in the bulk of the samples was $C_0 = 0$;
- D_{app} remained constant for a given sample;
- The hydrogen content was homogeneous for a given diffusion depth;
- There was no hydrogen trapping.

The theoretical Fick's law curves were drawn and the hydrogen diffusion coefficient was determined by dichotomy, using the maximal hydrogen penetration depth, d_H^{th} , as a parameter that should be optimised. The calculations were performed by trying to be as close as possible to the experimental hydrogen penetration depth, d_H^{exp} . On the theoretical

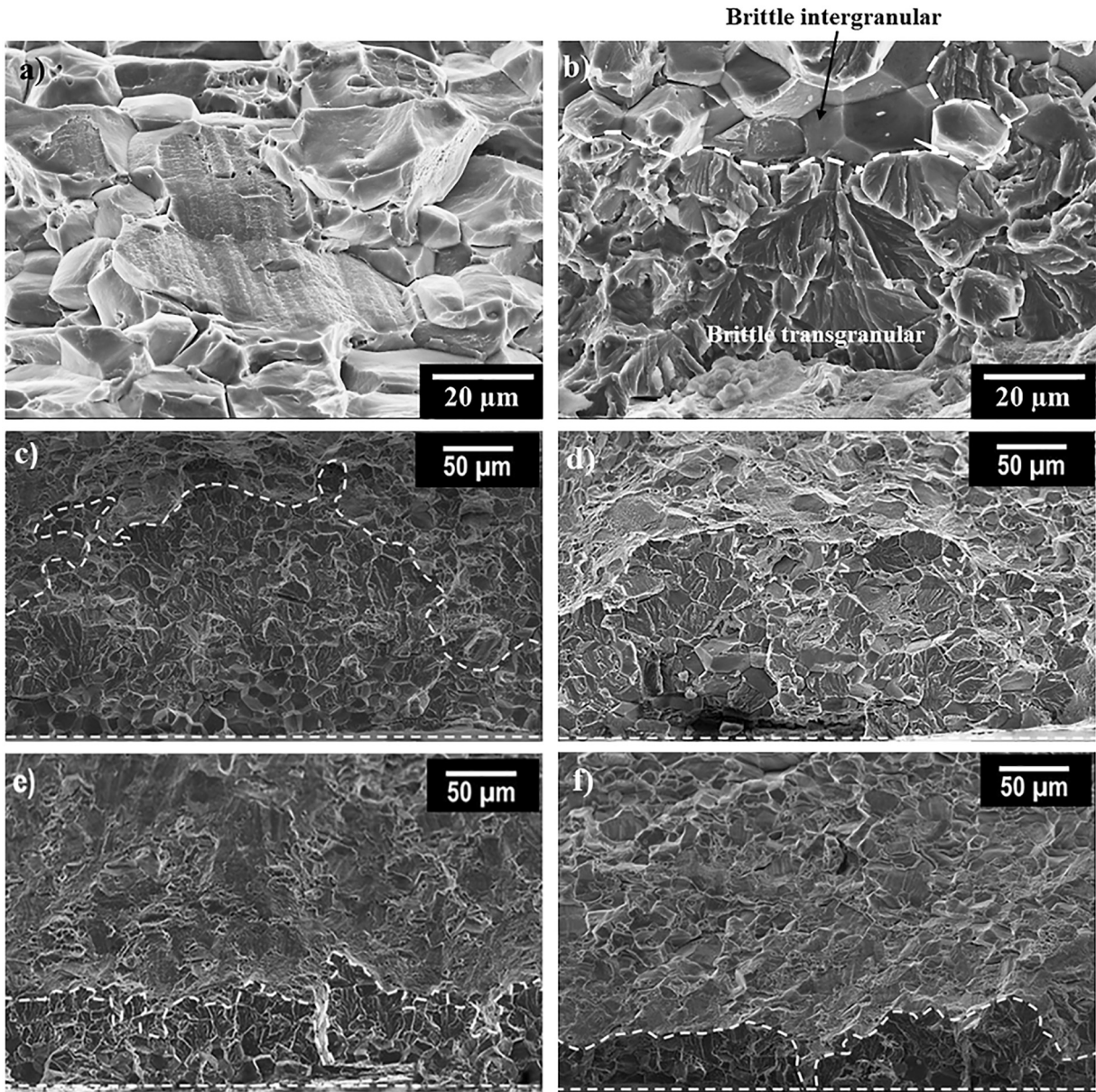


Fig. 5. SEM micrographs of the fracture surface for a non-pre-strained AA7046 sample after a 24 h-exposure to 0.6 M NaCl solution a) in the core of the samples, b) in the hydrogen-affected zone and c) global view. SEM micrographs of the brittle fracture zones for pre-strained samples after a 24 h-exposure to 0.6 M NaCl solution. The pre-strain level was 3% (d), 5% (e) and 7% (f).

curves, it was considered that d_H^{th} was reached when C_s decreased of 90%, i.e. when $c(x) < 0.1$ ($c(x)$ was the hydrogen concentration at a distance x from the hydrogen-charged surface).

$$\frac{c(x)-c_s}{c_0-c_s} = \operatorname{erf}\left(\frac{x}{2\sqrt{D_{app}t}}\right) \quad (2)$$

All calculated D_{app} values were summarised in Table 2 and confirmed a decrease in the hydrogen diffusion coefficient in the alloy when the pre-strain level increased. However, it was necessary to note that the values were of the same order of magnitude, which was consistent with all previous results. 16 measurement lines were systematically drawn simultaneously for each sample to improve the reliability of results. The differences measured could thus be considered as trustful, even though they corresponded to slight differences.

In their study, Scully et al. [12] studied the influence of various traps on the hydrogen diffusion in aluminium alloys. They showed that the vacancies had a stronger influence on hydrogen diffusion than the dislocations: a large number of dislocations were required to show a significant effect on the hydrogen diffusion. This was consistent with both:

- the fact that a high level of pre-straining was required to show an effect on the fracture surfaces of samples exposed to the chloride medium;
- the fact that the differences in the hydrogen penetration depths measured by SKPFM for the different pre-strained samples were less significant compared to what was observed in a previous work focussed on hydrogen – hardening precipitates interactions [22].

Following this idea, it was thus interesting to compare the evolution of the apparent hydrogen diffusion coefficient versus the dislocation

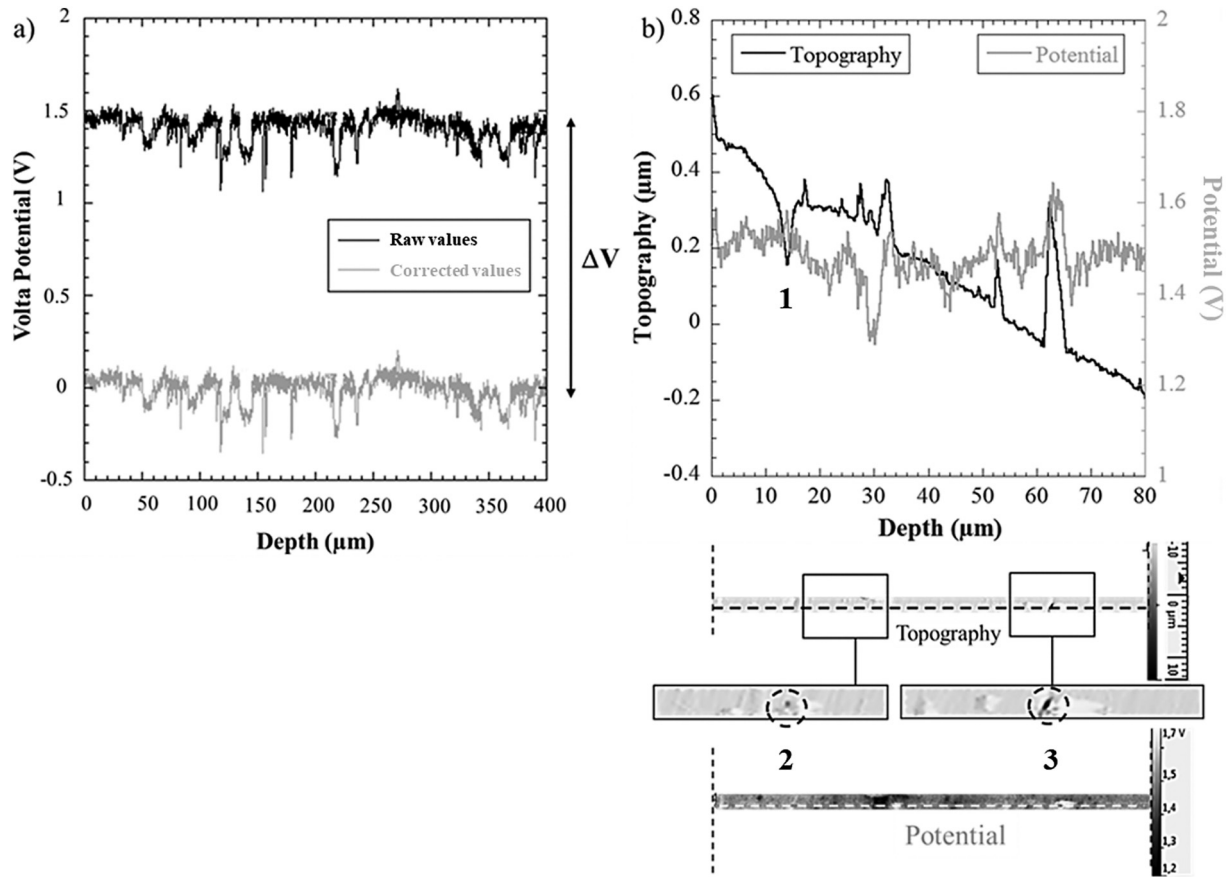


Fig. 6. a) Evolution of the Volta potential (V) as a function of the depth for an uncharged AA7046 T4 sample: the raw value (black curve) corresponds to the direct measurements and ΔV (gray curve) corresponds to the normalised values. Panel b) focuses on a 80 μm large area and shows the relationship between topography and potential.

densities calculated from XRD measurements as previously showed in Fig. 2. Fig. 8 showed similar behaviour considering the XRD measurements analysed with FP and LaB6 methods. Further, a D_{app} /dislocation density (ρ) relationship described by Eq. (3) was highlighted with C_1

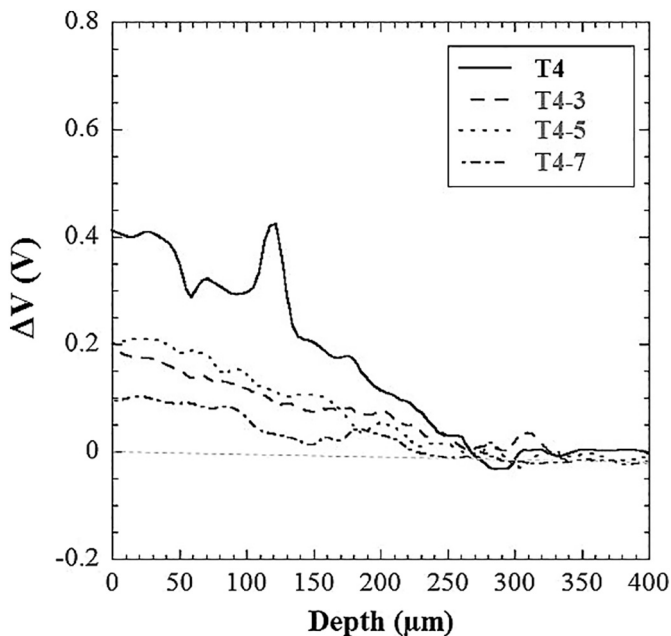


Fig. 7. SKPFM profiles plotted for AA7046-T4 cathodically hydrogen-charged in H_2SO_4 for 72 h. Samples with different pre-strain levels are compared.

and C_2 two constants:

$$D_{app} = \frac{1}{C_1 + C_2\rho} \quad (3)$$

This relationship could be related to other studies carried out by Young and Scully for aluminium alloys [37]. Indeed, to describe the influence of different trapping sites on D_{app} values, these authors proposed an equation (Eq. (4)). This last was based on the assumptions that (i) the number of interstitial sites, $N_{lattice}$, was high compared to the number of trapping sites, (ii) the hydrogen amount inserted in the alloy was negligible compared to the number of trapping sites, and (iii) that trap occupancy was close to zero. $D_{lattice}$ was the interstitial hydrogen diffusion coefficient, N_{trap} the number of one kind of trapping site (vacancy, dislocations, grain boundaries or precipitates) and E_b the binding energy depending on the trapping site. As a consequence, the influence of the traps on the hydrogen diffusion would be related to the equilibrium between the number of trapping sites and the number of interstitial sites and to the “strength” of the traps. As previously explained, Pressouyre [10] described the dislocations as reversible traps and thus apparently not really susceptible to affect hydrogen diffusion

Table 2

Hydrogen penetration depth measured by SKPFM and calculated apparent hydrogen diffusion coefficients for pre-strained and hydrogen-charged AA7046 samples.

Total strain (%)	Hydrogen penetration depth (μm)	D_{app} ($\text{m}^2 \cdot \text{s}^{-1}$)
0	275 ± 15	$(2.2 \pm 0.2) 10^{-14}$
3	240 ± 10	$(1.7 \pm 0.1) 10^{-14}$
5	220 ± 10	$(1.5 \pm 0.1) 10^{-14}$
7	210 ± 15	$(1.3 \pm 0.1) 10^{-14}$

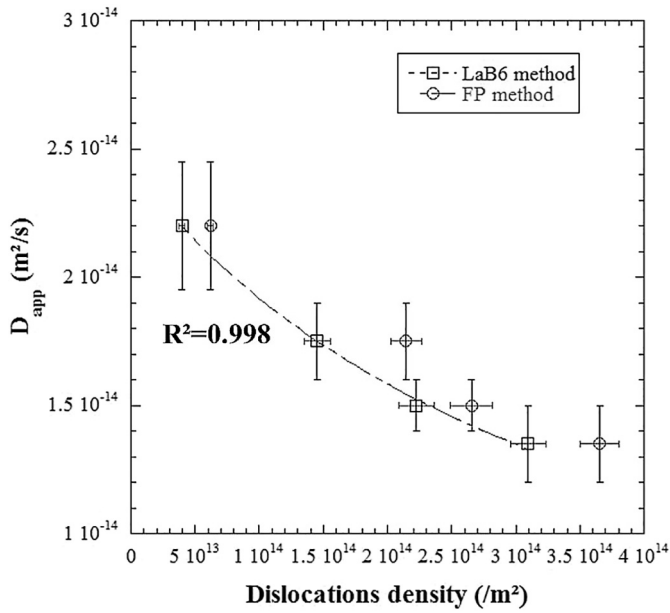


Fig. 8. Apparent hydrogen diffusion coefficient versus dislocation density for AA7046 samples hydrogen-charged in sulfuric acid and pre-strained prior hydrogen charging.

by a trapping effect. This could explain the need to drastically increase the total deformation of the samples in order to highlight a significant effect of the dislocations on the hydrogen diffusion.

$$D_{app} = \frac{D_{lattice}}{1 + \sum \frac{N_{trap}}{N_{lattice}} \exp\left(\frac{E_b}{RT}\right)} \quad (4)$$

The similarity between the behaviour proposed by Young and Scully and the experimental results obtained in this study improved the reliability of the results; it also strengthened the relationship between the hydrogen diffusion coefficient and the dislocation density. However, the exact role of dislocations is still discussed and the different assertions can be contradictory. Indeed, Saitoh et al. [38] studied the influence of different microstructural heterogeneities on the hydrogen diffusion. They used tritium autoradiography technique in pure aluminium and in solution-treated Al-Mg₂Si alloys to study the tritium distribution in pre-strained samples. EM autoradiographs revealed a heterogeneous distribution of the tritium which was mainly detected at the extremity of the dislocations. This suggested that two types of interactions had to be distinguished:

- The ability of dislocations to trap the hydrogen;
- The role of short-circuit diffusion that dislocations could play for hydrogen (explaining why the hydrogen was mainly observed at the end of the dislocations).

Indeed, the dislocations could be seen as trapping sites because of the lower potential energy of the hydrogen at a dislocation compared to the matrix; however, the lower potential energy along the dislocation lines allowed easier diffusion of the hydrogen across the dislocation network. Park et al. [39] showed, in EH 36 steel, for a 20% pre-strained sample, that motionless dislocations decreased D_{app} by approximately ten times and increased both the total hydrogen content and the amount of hydrogen trapped in reversible sites by approximately three times. For the authors, the dislocations would delay the motion of hydrogen.

In the present study, the results had to be discussed regarding these two considerations. Significant changes in the hydrogen diffusion coefficient and on the fracture surfaces were highlighted only for total pre-

straining of 5 and 7%. This could be explained by the complexity of the dislocation network. For T4-3 samples, the density of dislocations increased, but their ability to act as preferential paths for hydrogen made the trapping effect not visible at a macroscopic scale, even if hydrogen was trapped on dislocations. As a consequence, no differences were observed compared to the T4 reference sample on the fracture surfaces. Only the SKPFM measurements suggested that the hydrogen diffusion slightly decreased presumably due to the trapping. For higher pre-straining, the dislocation network in T4-5 and T4-7 samples was more complex and tangled. As a consequence, even if the dislocations could act as both, short-circuit diffusion and trapping sites, the tangle of dislocations increased the length of the path they formed. Indeed, at a macroscopic scale, only the trapping effect of the dislocations could be observed leading to both a decrease in the hydrogen diffusion coefficient and a change in the macroscopic fracture modes due to the distribution of hydrogen on different trapping sites, and especially on dislocations. Therefore, in T4-5 and T4-7 states, hydrogen was less susceptible to be found in grain boundaries. This phenomenon was also highlighted by a study of Kamoutsi et al. [11] who carried out thermal desorption spectroscopy measurements to characterise the distribution of hydrogen on the different trapping sites in a pre-strained AA2024. The experimental procedure used for the pre-strain stage was similar to the one used in the present study. The authors observed an increase in the hydrogen amount on dislocations up to a 6% strain level, which confirmed the increase in the amount of hydrogen trapped on dislocations and thus the present hypotheses.

The results obtained in this study were therefore consistent with the analysis proposed by Young and Scully, which contributed to confirm the efficiency of hydrogen trapping by dislocations. A deeper investigation of Eqs. (3) and (4) could be interesting but the hypotheses made to calculate C_1 and C_2 were too much limiting. At first, it was assumed that the hydrogen diffusion coefficient in the lattice ($D_{lattice}$) was similar for each pre-strained sample, which could not be confirmed because the increase in the dislocation density could induce distortions in the lattice and thus modify $D_{lattice}$. Then, it was assumed here that only the dislocation density was affected by the pre-strain stage whereas interfaces could be modified and vacancies could be created [40,41]. Furthermore, it is admitted that vacancies can act as hydrogen trapping sites characterised by a higher binding energy than dislocations [42], and strongly modify the hydrogen diffusion in the lattice. Lu et al. [43] studied the hydrogen-vacancies interactions by ab initio calculations. They showed that up to 12 hydrogen atoms could be trapped in vacancies and that the trapped hydrogen could promote the formation of vacancy clusters that were elsewhere considered as initiation sites for micro-cracks supporting HELP mechanism. Finally, Young and Scully showed a significant influence of vacancies on hydrogen diffusion and trapping in aluminium alloys, even at relatively low concentrations, whereas a large amount of dislocations was required for hydrogen trapping on dislocations to significantly affect the apparent diffusivity of the hydrogen [12]. An experimental determination of vacancy density in the alloy would thus be necessary to complete the analysis but this was not the focus of this study. It would be also necessary to determine the relationship between the number of dislocations and the number of traps, which is related to the Burger's vectors and thus to the nature of the dislocations to take into account the other traps [44].

4. Conclusions

The study focused on the interactions between motionless dislocations and hydrogen in an Al-Zn-Mg alloy. AA7046-T4 aluminium alloy was pre-strained by tensile tests at 3, 5 and 7% of total strain (i.e. elastic and plastic deformation). XRD measurements confirmed that the dislocation density increased with the increased strain level by two methods (FP and LaB6). First, exposure of the pre-strained samples in 0.6 M NaCl showed that the loss of elongation to failure attributed to hydrogen penetration inside the alloy was reduced when the dislocation density

increased. This was associated with a decrease in the fraction of surface area covered by brittle intergranular fracture on the fracture surfaces in favour of brittle transgranular fracture. The results were explained considering hydrogen trapping by dislocations that limited the hydrogen diffusion and decreased the hydrogen amount in the grain boundaries. This was confirmed by the calculations of apparent hydrogen diffusion coefficient on the basis of SKPFM measurements performed for pre-strained samples cathodically hydrogen-charged in sulfuric acid. In the future, it will be of interest to characterise the dislocation networks generated for low pre-strain levels. Moreover, the redistribution of the hydrogen trapped by precipitates and dislocations during the tensile tests, in particular due to the interactions between hydrogen and mobile dislocations, should be also taken into account. At last, the role of hydrogen-vacancy interactions on hydrogen diffusion/trapping and vacancy saturation should be considered to improve the first approach proposed in the present work.

Data statement

Data are available if requested.

CRedit authorship contribution statement

L. Oger: Investigation, Methodology, Writing - original draft. **B. Malard:** Methodology. **G. Odemer:** Methodology, Supervision, Writing - review & editing. **L. Peguet:** Funding acquisition, Resources. **C. Blanc:** Methodology, Funding acquisition, Project administration, Supervision, Validation, Writing - review & editing.

Acknowledgments

The authors thank Constellation Technology Center (Voreppe, France) for its financial support. They also thank Rémi Garcia for XRD measurements and Tanguy Manescau, Colette Perez and Aline Valleau for the work they performed during their 2nd year laboratory project.

References

- [1] L. Marretta, R. Di Lorenzo, F. Micari, J. Arinez, D. Dornfeld, Material substitution for automotive applications: a comparative life cycle analysis, *Leveraging Technol. a Sustain. World Proc. 19th CIRP Conf. Life Cycle Eng. Univ. Calif. Berkeley, Berkeley, USA, May 23–25, 2012* 2012, pp. 61–66, https://doi.org/10.1007/978-3-642-29069-5_11.
- [2] S. Dey, I. Chatteraj, Interaction of strain rate and hydrogen input on the embrittlement of 7075 T6 aluminum alloy, *Mater. Sci. Eng. A* 661 (2016) 168–178, <https://doi.org/10.1016/j.msea.2016.03.010>.
- [3] N.J.H. Holroyd, G.M. Scamans, Stress corrosion cracking in Al-Zn-Mg-Cu aluminum alloys in saline environments, *Metall. Mater. Trans. A Phys. Metall. Mater. Sci.* 44 (2013) 1230–1253, <https://doi.org/10.1007/s11661-012-1528-3>.
- [4] A.C.U. Rao, V. Vasu, M. Govindaraju, K.V.S. Srinadh, Stress corrosion cracking behaviour of 7xxx aluminum alloys: a literature review, *Trans. Nonferrous Metals Soc. China* 26 (2016) 1447–1471, [https://doi.org/10.1016/S1003-6326\(16\)64220-6](https://doi.org/10.1016/S1003-6326(16)64220-6).
- [5] D. Najjar, T. Magnin, T. Warner, Influence of critical surface defects and localized competition between anodic dissolution and hydrogen effects during stress corrosion cracking of a 7050 aluminium alloy, *Mater. Sci. Eng. A* 238 (1997) 293–302, [https://doi.org/10.1016/S0921-5093\(97\)00369-9](https://doi.org/10.1016/S0921-5093(97)00369-9).
- [6] M. Ajay Krishnan, V.S. Raja, Role of temper conditions on the hydrogen embrittlement behavior of AA 7010, *Corros. Sci.* 152 (2019) 211–217, <https://doi.org/10.1016/j.corsci.2019.03.004>.
- [7] D. Najjar, *Compétition entre les mécanismes de dissolution anodique et de fragilisation par l'hydrogène dans le processus de fissuration par corrosion sous contrainte de l'alliage Al-Zn-Mg-Cu 7150 sollicité en traction lente en milieu chloruré (NaCl 3%), 1994.*
- [8] G.M. Scamans, R. Alani, P.R. Swann, Pre-exposure embrittlement and stress corrosion failure in AlZnMg Alloys, *Corros. Sci.* 16 (1976) 443–459, [https://doi.org/10.1016/0010-938X\(76\)90065-2](https://doi.org/10.1016/0010-938X(76)90065-2).
- [9] Md. Shahnewaz Bhuiyan, Y. Toda, H. Toda, S. Hang, K. Uesugi, A. Takeuchi, N. Sakaguchi, Y. Watanabe, Influence of hydrogen on deformation and fracture behaviors of high Zn 7xxx aluminum alloys, *Int. J. Fract.* 200 (2016) 13–29, <https://doi.org/10.1007/s10704-016-0092-z>.
- [10] G.M. Pressouyre, A classification of hydrogen traps in steel, *Metall. Trans. A* 10 (1979) 1571–1573, <https://doi.org/10.1007/BF02812023>.
- [11] H. Kamoutsi, G.N. Haidemenopoulos, V. Bontozoglou, P.V. Petroyiannis, S.G. Pantelakis, Effect of prior deformation and heat treatment on the corrosion-induced hydrogen trapping in aluminium alloy 2024, *Corros. Sci.* 80 (2014) 139–142, <https://doi.org/10.1016/j.corsci.2013.11.021>.
- [12] G.A. Young, J.R. Scully, The diffusion and trapping of hydrogen in high purity aluminium, *Acta Metall.* 18 (1998) 6337–6349, [https://doi.org/10.1016/0001-6160\(70\)90078-7](https://doi.org/10.1016/0001-6160(70)90078-7).
- [13] M.O. Speidel, *Hydrogen embrittlement and stress-corrosion cracking of aluminum alloys*, in: R. Gibala, R.F. Hehemann (Eds.), *Hydrogen Embrittlement and Stress-Corrosion Cracking*, Amer. Soc. Met, Metals Park 1984, pp. 271–297.
- [14] Md. Shahnewaz Bhuiyan, H. Toda, Z. Peng, S. Hang, K. Horikawa, K. Uesugi, A. Takeuchi, N. Sakaguchi, Y. Watanabe, Combined microtomography, thermal desorption spectroscopy, X-ray diffraction study of hydrogen trapping behavior in 7XXX aluminum alloys, *Mater. Sci. Eng. A* 655 (2016) 221–228, <https://doi.org/10.1016/j.msea.2015.12.092>.
- [15] S.P. Lynch, Comments on “A unified model of environment-assisted cracking”, *Scr. Mater.* 61 (2009) 331–334, <https://doi.org/10.1016/j.scriptamat.2009.02.031>.
- [16] C.D. Beachem, A new model for hydrogen-assisted cracking (hydrogen “embrittlement”), *Metall. Trans. A* 3 (1972) 441–455, <https://doi.org/10.1007/BF02642048>.
- [17] I.M. Robertson, The effect of hydrogen on dislocation dynamics, *Eng. Fract. Mech.* 68 (2001) 671–692, [https://doi.org/10.1016/S0013-7944\(01\)00011-X](https://doi.org/10.1016/S0013-7944(01)00011-X).
- [18] G.M. Bond, I.M. Robertson, H.K. Birnbaum, The influence of hydrogen on deformation and fracture processes in high-strength aluminum alloys, *Acta Metall.* 35 (1987) 2289–2296, [https://doi.org/10.1016/0001-6160\(89\)90234-4](https://doi.org/10.1016/0001-6160(89)90234-4).
- [19] G. Bond, I. Robertson, H. Birnbaum, Effects of hydrogen on deformation and fracture processes in high-purity aluminium, *Acta Metall.* 36 (1988) 2193–2197, [https://doi.org/10.1016/0001-6160\(88\)90320-3](https://doi.org/10.1016/0001-6160(88)90320-3).
- [20] P.J. Ferreira, I.M. Robertson, H.K. Birnbaum, Hydrogen effects on the character of dislocations in high-purity aluminum, *Acta Mater.* 47 (1999) 2991–2998, [https://doi.org/10.1016/S1359-6454\(99\)00156-1](https://doi.org/10.1016/S1359-6454(99)00156-1).
- [21] H. Sua, H. Toda, R. Masunaga, K. Shimizu, H. Gao, K. Sasaki, Md. Shahnewaz Bhuiyan, K. Uesugi, A. Takeuchi, Y. Watanabe, Influence of hydrogen on strain localization and fracture behavior in Al-Zn-Mg-Cu aluminum alloys, *Acta Mater.* 159 (2018) 332–343, <https://doi.org/10.1016/j.actamat.2018.08.024>.
- [22] L. Oger, M.C. Lafouresse, G. Odemer, L. Peguet, C. Blanc, Hydrogen diffusion and trapping in a low copper 7xxx aluminium alloy investigated by Scanning Kelvin Probe Force Microscopy, *Mater. Sci. Eng. A* 706 (2017) 126–135, <https://doi.org/10.1016/j.msea.2017.08.119>.
- [23] C. Larignon, J. Alexis, E. Andrieu, L. Lacroix, G. Odemer, C. Blanc, Investigation of Kelvin probe force microscopy efficiency for the detection of hydrogen ingress by cathodic charging in an aluminium alloy, *Scr. Mater.* 68 (2013) 479–482, <https://doi.org/10.1016/j.scriptamat.2012.11.026>.
- [24] S. Evers, C. Senöz, M. Rohwerder, Spatially resolved high sensitive measurement of hydrogen permeation by scanning Kelvin probe microscopy, *Electrochim. Acta* 110 (2013) 534–538, <https://doi.org/10.1016/j.electacta.2013.04.171>.
- [25] M. Koyama, A. Bashir, M. Rohwerder, S.V. Merzlikin, E. Akiyama, K. Tsuzaki, D. Raabe, Spatially and kinetically resolved mapping of hydrogen in a twinning-induced plasticity steel by use of scanning Kelvin probe force microscopy, *J. Electrochem. Soc.* 162 (2015) C638–C647, <https://doi.org/10.1149/2.0131512jes>.
- [26] M.C. Lafouresse, M.-L. de Bonfils-Lahovary, C. Charvillat, L. Oger, L. Laffont, C. Blanc, A Kelvin probe force microscopy study of hydrogen insertion and desorption into 2024 aluminum alloy, *J. Alloys Compd.* 722 (2017) 760–766, <https://doi.org/10.1016/j.jallcom.2017.06.143>.
- [27] M. Nonnenmacher, M.P. O'Boyle, H.K. Wickramasinghe, Kelvin probe force microscopy, *Appl. Phys. Lett.* 58 (1991) 2921–2923, <https://doi.org/10.1063/1.105227>.
- [28] C. Senöz, S. Evers, M. Stratmann, M. Rohwerder, Scanning Kelvin Probe as a highly sensitive tool for detecting hydrogen permeation with high local resolution, *Electrochem. Commun.* 13 (2011) 1542–1545, <https://doi.org/10.1016/j.elecom.2011.10.014>.
- [29] Bruker, *TOPAS V3: general profile and structure analysis software for powder diffraction data, User's Manual, Bruker AXS, Karlsruhe, Ger., 2005*
- [30] H.M. Rietveld, A profile refinement method for nuclear and magnetic structures, *J. Appl. Crystallogr.* 2 (1969) 65–71, <https://doi.org/10.1107/S0021889869006558>.
- [31] S. Hata, H. Miyazaki, S. Miyazaki, M. Mitsuhashi, M. Tanaka, K. Kaneko, K. Higashida, K. Ikeda, Ultramicroscopy high-angle triple-axis specimen holder for three-dimensional diffraction contrast imaging in transmission electron microscopy, *Ultramicroscopy* 111 (2011) 1168–1175, <https://doi.org/10.1016/j.ultramic.2011.03.021>.
- [32] G.K. Williamson, R.E. Smallman, Dislocation densities in some annealed and cold-worked metals from measurements on the X-Ray Debye-Scherrer Spectrum, *Philos. Mag.* 1 (1956) 34–45, <https://doi.org/10.1080/14786435608238074>.
- [33] G.K. Williamson, R.E. Smallman, The use of Fourier analysis in the interpretation of X-ray line broadening from cold-worked iron and molybdenum, *Acta Crystallogr.* 7 (1954) 574–581, <https://doi.org/10.1107/S0365110X54001879>.
- [34] H. Adachi, Y. Miyajima, M. Sato, N. Tsuji, Evaluation of dislocation density for 1100 aluminum with different grain size during tensile deformation by using in-situ X-ray diffraction technique, *Mater. Trans.* 56 (2015) 671–678, <https://doi.org/10.2320/matertrans.L-M2015803>.
- [35] G. Dini, R. Ueji, A. Najafzadeh, S.M. Monir-Vaghefi, Flow stress analysis of TWIP steel via the XRD measurement of dislocation density, *Mater. Sci. Eng. A* 527 (2010) 2759–2763, <https://doi.org/10.1016/j.msea.2010.01.033>.
- [36] J. Fusy, B. Bigeard, A. Cassuto, Etude de l'adsorption de l'oxygène sur ruban de rhénium par mesure des variations du travail d'extraction électronique, *Surf. Sci.* 46 (1974) 177–187.
- [37] J.R. Scully, G.A. Young Jr, S.W. Smith, Hydrogen solubility, diffusion and trapping in high purity aluminum and selected Al-base alloys, *Mater. Sci. Forum* 331–337 (2000) 1583–1600, <https://doi.org/10.4028/www.scientific.net/MSF.331-337.1583>.

- [38] H. Saitoh, Y. Iijima, K. Hirano, Behaviour of hydrogen in pure aluminium, Al-4 mass% Cu and Al-1 mass% Mg2Si alloys studied by tritium electron microautoradiography, *J. Mater. Sci.* 29 (1994) 5739–5744, <https://doi.org/10.1007/BF00349974>.
- [39] C. Park, N. Kang, M. Kim, S. Liu, Effect of prestrain on hydrogen diffusion and trapping in structural steel, *Mater. Lett.* 235 (2019) 193–196, <https://doi.org/10.1016/j.matlet.2018.10.049>.
- [40] C. Panseri, F. Gatto, T. Federighi, Interaction between solute magnesium atoms and vacancies in aluminium, *Acta Metall.* 6 (1958) 198–204.
- [41] G. Saada, Les défauts ponctuels produits par écrouissage dans les métaux, *J. Phys.* 24 (1963) 426.
- [42] M. Nagumo, K. Takai, The predominant role of strain-induced vacancies in hydrogen embrittlement of steels: overview, *Acta Mater.* 165 (2019) 722–733, <https://doi.org/10.1016/j.actamat.2018.12.013>.
- [43] G. Lu, E. Kaxiras, Hydrogen embrittlement of aluminum: the crucial role of vacancies, *Phys. Rev. Lett.* 94 (2005) 1–4, <https://doi.org/10.1103/PhysRevLett.94.155501>.
- [44] T. Lu, Y.-P. Xu, X.-D. Pan, H.-S. Zhou, F. Ding, Z. Yang, G.-J. Niu, G.-N. Luo, X.-C. Li, F. Gao, Atomistic study of hydrogen behavior around dislocations in α iron, *J. Nucl. Mater.* 510 (2018) 219–228, <https://doi.org/10.1016/j.jnucmat.2018.08.018>.